Impact of Grid Refinement on Turbulent Combustion and Combustion Noise Modeling with Large Eddy Simulation

Feichi Zhang, Henning Bonart, Peter Habisreuther, and Henning Bockhorn

Abstract For Large Eddy Simulation (LES) of turbulent combustion, as the turbulent flow as well as the thin flame front are directly filtered by the cut-off scale, resolution of the computational grid plays a very important role in this case and represents always a quality determining factor. In addition, the fluctuation of heat release is found to be the main source for noise generation from turbulent combustion, which is attributed to the interaction of the turbulent flow and the combustion reaction. As the flame is thickened or filtered respectively by the computational grid, it becomes less sensitive to fluctuations of the flow as well, so that the emitted noise from the flame due to unsteady heat release is affected by the grid resolution in LES combustion modeling as well. The current work represents an investigation with respect to these aspects. For this purpose, LES and DNS simulations for a realistic jet flame at moderately turbulent condition have been carried out. The LES calculations have been performed on computational grids with different resolutions (0.4/3.2/10.7 million cells) on the HP XC4000 cluster of the Steinbuch Centre for Computing (SCC) at the KIT. In order to assess predictability of the LES methodology, a three-dimensional DNS simulation on a grid with 54 million cells has been carried out on the Cray XE6 (HERMIT) of the High Performance Computing Center Stuttgart (HLRS). The comparison of the LES solution with experimental and DNS data allows an evaluation of the influence of the grid refinement to a great extent.

F. Zhang (✉) · H. Bonart · P. Habisreuther · H. Bockhorn
Division of Combustion Technology, Engler-Bunte-Institute, Karlsruhe Institute of Technology, Engler-Bunte-Ring 1, 76131 Karlsruhe, Germany
e-mail: feichi.zhang@kit.edu

W.E. Nagel et al. (eds.), *High Performance Computing in Science and Engineering '13*, DOI 10.1007/978-3-319-02165-2_19,
© Springer International Publishing Switzerland 2013

1 Introduction

Large eddy simulation (LES) has become a popular method for numerical modeling of turbulent combustion flows in recent years. This is attributed to the need for more predictive simulation methods and the tremendous progress in computational powers. Combustion in practical devices usually occurs with a fast mixing progress and a short reaction time, so that stabilization of the flame generally takes place in very complicated flow patterns, such as swirling flows, breakdowns of large-scale vortical structures, and recirculation regions. For this case, the traditional Reynolds-averaged Navier-Stokes (RANS) method often cannot satisfy the required accuracy [1]. In LES, the turbulent flow field is divided into a large-scale resolved and a small-scale unresolved contribution. This is done by spatially filtering the field variables, hence, removing turbulent motions of length scales smaller than the filter size. Compared to the conventional RANS models, LES is more expensive in computational cost. The advantage of LES is however that the large-scale energy containing motion of the turbulence is resolved directly, whereas the small-scale vortices exhibit more universal features and modeling of these fine structures is more suited [2].

For numerical computation of combustion noise, the hybrid CFD (Computational Fluid Dynamics)/CAA (Computational Aero-Acoustics) method remains as the most commonly used tool until now [3]. In this technique, the noise-generating acoustic sources (e.g. the turbulent flame) are calculated with help of CFD combustion modeling, which serve as input data for the subsequent CAA computation to describe propagations of sound waves emitted from these noise sources into the far field [4]. On the other side, the acoustic radiation from a turbulent flame can be obtained by solving the compressible Navier-Stokes (NS) equations directly, for example, in framework of a DNS (Direct Numerical Simulation) or a LES. The major shortcoming of these concepts is that the computational domain is often restricted to a relatively small region close to the flame to reduce computational cost which would be very high in case of using a large domain due to the disparity between the length scales of the reactive flow (thickness of a flame $O(\delta_f) \cong 0.1\,\text{mm}$) and the propagating acoustic waves (wave length in the far field $O(\lambda) \cong 1\,\text{m}$).

In comparison with the conventional modeling methodologies like RANS or LES, the application of DNS for combustion related problems is mainly limited to research purpose, for example, for flows with a very low Reynolds number (Re) or restricted to a small and simple computational domain, due to a very high computational effort. On the other hand, a DNS solves the governing equations exactly without any empirical models and provides a detailed insight into the interaction of the turbulent flow with the chemical kinetics, so that it can be used to validate and to improve subordinate modeling methods.

2 Combustion Modeling

The current work applies an extended version of the reaction model of Schmid et al. [5] to describe the combustion reaction and its interaction with the turbulent flow. The concept makes use of the progress variable θ to follow the combustion reaction progress, which is defined in our work by means of the chemically bounded oxygen. It quantifies the transition from unburnt ($\theta = 0$) to burnt state ($\theta = 1$) by:

$$\theta = \frac{y_{O_2} - y_{O_2,ub}}{y_{O_2,br} - y_{O_2,ub}} \tag{1}$$

In (1), $y_{O_2,ub}$ and $y_{O_2,br}$ indicate mass fractions of O_2 in the unburnt and the completely burnt state (of equilibrium). The LES averaged formulation of the transport equation for θ is given as [6]:

$$\frac{\partial \bar{\rho}\tilde{\theta}}{\partial t} + \frac{\partial \bar{\rho}\widetilde{u_i}\tilde{\theta}}{\partial x_i} = \frac{\partial}{\partial x_i}\left(\frac{\mu_l + \mu_t}{Sc_t}\frac{\partial \tilde{\theta}}{\partial x_i}\right) + \bar{\dot{\omega}}_\theta \tag{2}$$

where $\bar{\cdot}$ denotes a spatially filtered value and $\tilde{\cdot}$ a Favre-filtered value. The turbulent flame speed S_t in the source term, $\bar{\dot{\omega}}_\theta$ has to be modeled to close the equation mathematically. For this reason, it belongs to the class of turbulent flame-speed closure (TFC) combustion models [6]. The rate term in (2) is given as follows [5]:

$$\bar{\dot{\omega}}_\theta = \rho_u \frac{S_t^2}{D_l + D_t}\tilde{\theta}(1 - \tilde{\theta}), \quad \frac{S_t}{S_l} = 1 + \frac{u'}{S_l}\left(1 + Da^{-2}\right)^{-1/4} \tag{3}$$

with the laminar burning velocity S_l, the density of the unburnt mixture ρ_u, the turbulence intensity u' and the turbulent length scale L_t. D_l and D_t are the laminar and turbulent diffusion coefficient which are related to the laminar and turbulent viscosities through the Schmidt number; the Dahmköhler number Da is evaluated by the ratio of the turbulent time scale $\tau_t = L_t/u'$ to the chemical time scale $\tau_c \propto a/S_l^2$ with the thermal diffusivity a.

To account for mixing effects, a transport equation for the mixture fraction ξ is solved additionally. Assuming that the mixing of fuel and oxidizer takes place before the chemical reaction, the entire turbulent flame can be considered as an ensemble of distinct reaction zones with different equivalence ratios. Thereby, the mixing process is controlled by the mixture fraction and the subsequent chemical reaction by the progress variable. Structures of the individual premixed reaction layers can then be pre-computed by solving 1D flame equations, for example, using the CHEMKIN program package [7]. To take the effect of turbulence on mixing into account, the pre-defined profiles of these flame sheets are averaged by a probability density function (PDF) $P(\xi)$ determined by the mean value of $\tilde{\xi}$ and its variance $\widetilde{\xi''^2}$ with a presumed principal shape of a β-function [8]. Finally, all averaged (i.e. over the PDF integrated) quantities are picked up in a look-up table depending on the three control parameters: $\tilde{\xi}$, $\widetilde{\xi''^2}$ and $\tilde{\theta}$.

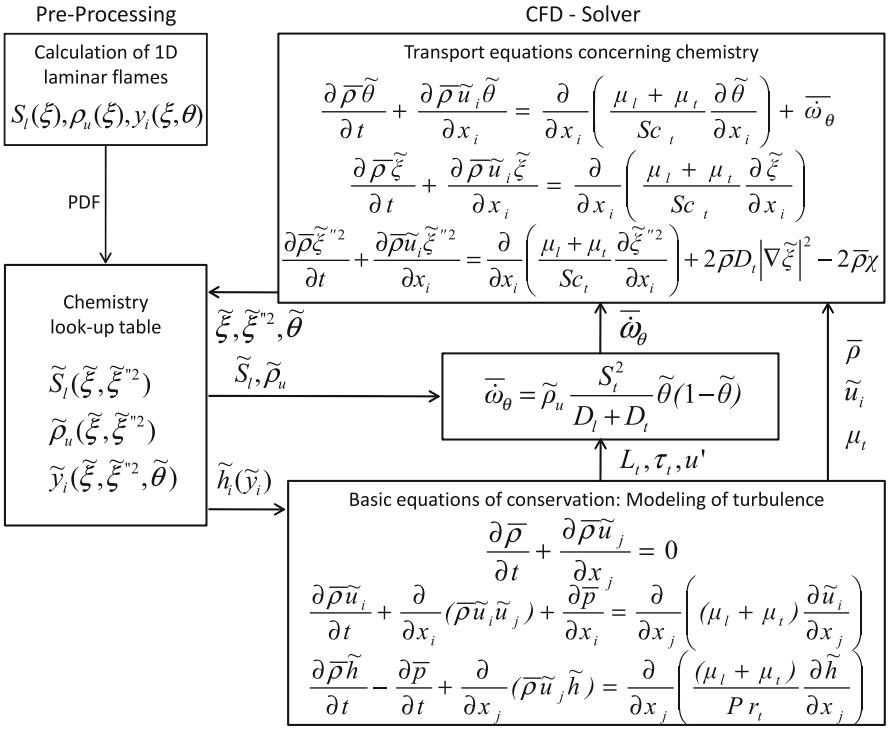

Fig. 1 Schematic of the link between the look-up chemistry table with the CFD solver

As illustrated in Fig. 1, internal structures of the reaction zones at different equivalence ratios are calculated in a pre-processing step with a detailed reaction mechanism. The flow solver and the pre-computed flame profiles, i.e. the look-up chemistry table, are linked through exchange of $\tilde{\xi}$, $\widetilde{\xi''^2}$ and $\tilde{\theta}$, where multi-dimensional interpolations have been applied in order to obtain intermediate values. The source term of the variance transport equation $\bar{\dot{\omega}}_{\xi''^2}$ is given by [8]:

$$\bar{\dot{\omega}}_{\xi''^2} = 2\bar{\rho}D_t|\nabla\tilde{\xi}|^2 - 2\bar{\rho}\tilde{\chi} \tag{4}$$

with the scalar dissipation rate $\tilde{\chi} \propto 1/\tau_t$.

To use the concept for LES combustion modeling, the turbulence parameters in S_t (i.e. u', τ_t and L_t) have been evaluated at the cut-off scale [9]. In doing so, the unresolved scalar flux increases the flame thickness, either through the turbulent or numerical diffusion, so that the thickened (implicitly filtered) flame front can be resolved on the LES mesh. Applications of the concept in connection with LES and RANS turbulence models have already been successfully performed for different flame regimes and validated by experiments [10, 11] so that it may be adequately used for the current study.

For DNS simulation, the three-dimensional conservation equations for total mass, momentum, energy and species masses, have been directly solved without using any simplifications. These constitute a large number of non-linear, partial differential equations which have to be solved numerically together with the thermodynamic equation of state. The reaction rates for the species equations are thereby calculated by means of the kinetic law of chemical reactions together with the extended Arrhenius law, whereas the ordinary species flux is given either by an exact but very time-consuming multi-component or a simplified mixture-averaged diffusion approach [12]. The molecular viscous and heat fluxes are evaluated with the exact transport coefficients.

3 Experimental and Numerical Setups

3.1 Case Description

The burner system shown in Fig. 2 has been designed and built at the Technische Universität Berlin in order to experimentally investigate the combustion-induced noise [13]. Therefore, its setup is deliberately kept simple by having an annular injector at the very bottom, a mixing plenum, a converging nozzle, and a cooled plate at the outlet of the nozzle. In order to reduce computational efforts even further, the Bunsen-type flame is stabilized by flame propagation itself. After fuel and air are well mixed in the plenum, the mixture flows through the nozzle and leaves the burner at the diameter D. The flame is then operated at atmospheric pressure and temperature, employing pure methane as fuel and the equivalence ratio $\phi = 1.3$ (fuel-rich). By passing through the nozzle, the flow accelerates yielding a Reynolds number of $Re = 7,500$ at the exit plane of the burner. Particle Image Velocimetry (PIV) and microphone measurements in an anechoic environment have been carried out for investigations of the flow field and the acoustic field, respectively.

3.2 Numerical Setups

As the considered case is represented by a round jet configuration, the computational domain is chosen to be constructed with the convergent nozzle part to allow development of the turbulence within the burner and the velocity changes directly at the nozzle exit, and a large cylindrical domain ($length \times diameter = 60D \times 90D$) downstream of the burner where mixing and combustion take place. Due to the simple geometries of the computational domain and in order to achieve best accuracy, the computational grids are built up in a block-structured way employing hexahedral shaped elements, as illustrated in Fig. 3. To study the effect of grid resolution on the LES combustion modeling, meshes with different refinements (but the same topology) have been conducted with 0.4/3.2/10.7 million cells. These are

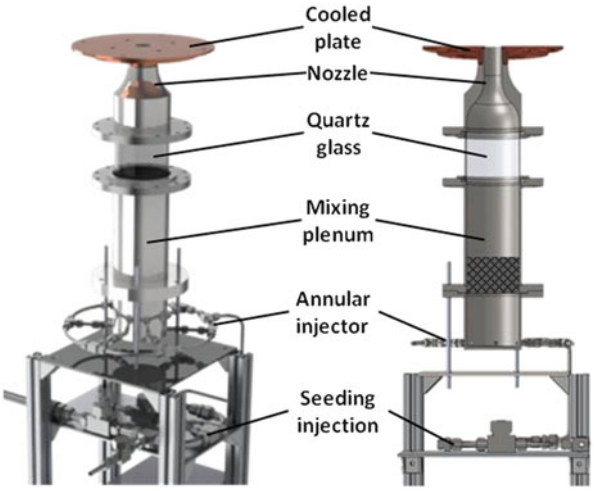

Fig. 2 Schematic of the experimental setup of the burner system [13]

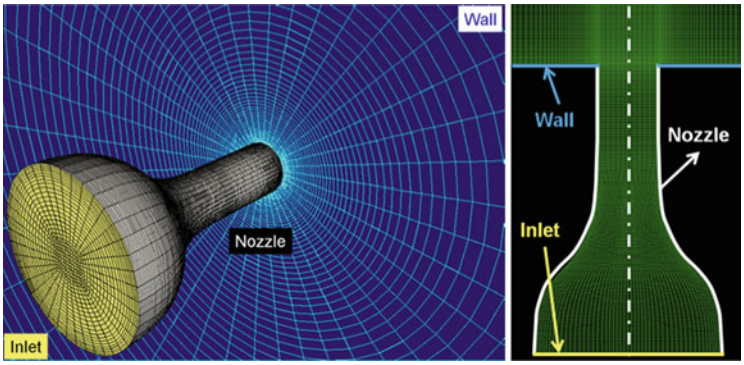

Fig. 3 Computational grid used for the LES

systematically refined along the burner wall and the shear layer continuously to a higher ordered refinement level. The smallest mesh sizes used for these critical regions are (from the coarsest to the finest grid) 0.7, 0.35, 0.175 mm. The x- and r-coordinates indicate always the streamwise and radial axis of the cylindrical coordinate system.

The DNS simulation has been restricted to a compact domain close to the flame ($length \times diameter = 23D \times 23D$) in order to save computational time. The computational grid is built up by approx. 54 million finite volumes. The smallest mesh size of 0.1 mm is used to resolve the reaction zone and the shear layer. The ordinary diffusion flux is described by the mixture-averaged approach and the combustion reaction covers a complex chemical mechanism with 18 species and 69 elementary reactions including the reaction chain of the short-lived OH^* free radical [14].

The open source CFD code OpenFOAM [15] has been used to solve the filtered and the exact conservation equations in LES and DNS, employing the finite volume method with a cell-centered storage arrangement. A fully implicit compressible formulation was applied together with the pressure-implicit split-operator (PISO) technique for the pressure correction [16]. Discretisation of convective flux terms is based on a second order interpolation scheme. The boundary conditions have been set according to the experimental setup, i.e. methane/air mixture of the equivalence ration of $\phi = 1.3$ flows from the inlet into the computational domain and becomes burnt after the convergent nozzle by a Re of 7,500 under atmospheric condition.

A turbulence inflow generator [17] was implemented in OpenFOAM and used for the LES and DNS simulations, which is based on digital filtering of random data series with pre-defined correlation functions. By doing so, it provides transiently correlated velocity components at the inlet boundary for each time step. The turbulence properties thereby was set according to LDA measurement of the velocity field within the quartz glass (see Fig. 2). The partially non-reflecting boundary condition (NRBC) proposed by Poinsot and Lele [18] has been applied to all inlet, outlet and entrainment boundaries in order to avoid unphysical reflection of pressure waves. One additional issue of the simulations is to include the buoyant force caused by the large density change through the flame front. As density of the unburnt mixture upstream of the flame front is much higher than that of the burnt mixture, the fresh gas upstream of the flame front is heavier than the hot product gas, leading to an upwardly buoyant force. The effect of buoyancy can be neglected for combustion at high Re as it causes only minor difference in that case. As the Re is relatively low in the current case, an acceleration of the flow through buoyant force is discernible in addition to the thermal expansion.

The combustion model proposed in Sect. 2 has been implemented into the OpenFOAM code, which was used together with the Smagorinsky subgrid scale (sgs) model [2] for LES combustion modeling, assuming a constant turbulent Schmidt/Prandtl number $Sc_t = Pr_t = 0.7$. For the LES modeling the CHEMKIN program package [7] has been used to calculate the internal flame structure applying the GRI 3.0 (Gas Research Institute) mechanism containing 325 reactions and 53 species [24] for methane/air combustion. The Implementation of the DNS solver is based on coupling the standard OpenFOAM applications with the thermo-chemical libraries of Cantera [19]. The OpenFOAM based program is thereby used for solving the governing equations together with the state equation in parallel, whereas the thermodynamic state in terms of pressure, temperature and species compositions, serves as input for the Cantera algorithms, which evaluate the necessary transport properties (e.g. viscosity, diffusion coefficients and thermal conductivity) and the reaction rates needed for solution of the conservation equations in OpenFOAM [20, 21].

3.3 Computational Effort and Performance

The LES on the coarsest grid with 0.4 mil. nodes has been made parallel with eight CPU cores (i7-860) on the in-house Beowulf Linux cluster at the Division

Table 1 Mesh parameters and simulation setups used for LES and DNS simulations

CFD	No. cells	Δ_{min} (mm)	N_{inlet}	Δt (μs)	t_{total} (s)	$N_{\Delta t}$	No. cores	$t_{clock}/\Delta t$ (s)	Core hours
LES	0.4 mil.	0.700	513	50	8	160.000	8 (BEOWULF)	2.5	900
LES	3.2 mil.	0.350	2,052	25	4	160.000	256 (XC4000)	2.0	23.000
LES	10.7 mil.	0.175	5,700	10	2.4	240.000	512 (XC4000)	2.5	85.000
DNS	53.9 mil.	0.1	19,305	2	0.2	100.000	8192 (CRAY)	10	2.3 mil.

of Combustion Technology in KIT. As the own cluster applies a Gigabit Ethernet Interconnect between the nodes, it is not able to speed up efficiently by increasing used number of processors. For this reason, the LES simulations on the finer grids (with 3.2 mil. and 10.7 mil. grid points) have been conducted on the HP XC4000 cluster of the Steinbuch Centre for Computing (SCC) at the KIT [22]. As the computational cost for DNS is much higher than that needed for LES, the DNS simulation has been carried out on the Cray XE6 (HERMIT) cluster in HLRS [23] with 8,192 cores. A total computing time of approx. 12 days has been conducted for 100.000 time steps.

Table 1 gives an overview on simulation setups used for the different cases, thereby Δ_{min} denotes the minimum mesh size applied for each computational grids and N_{inlet} indicates the used number of elements to resolve the inlet boundary patch. In order to obtain a temporally well resolved progress of the field variables and to fulfill the criterion of numerical stability, time steps Δt for the LES simulations were set to allow the overall CFL no. (Courant-Friedrichs-Lewy condition) to be below 0.2. After running the LES for some volumetric residence (or through flow) times, statistical averaging of the flow variables and sampling of the sound signals have been conducted over a certain simulation time of t_{total}. The number of processors used for LES on the HP XC4000 Cluster in SCC at KIT are typically chosen to run a whole simulation with less than two jobs using the maximal running time of 4,320 min. For LES simulations considered for the current work, where at least 100.000 time steps are necessary to get well averaged statistics, up to 512 processors are needed depending on the mesh size to achieve a computing speed of approximately 2.5 s per time step. Comparing performances of the LES calculations with 3.2 mil. and 10.7 mil. cells on the HP XC4000 cluster, the speedup is higher by using the finer mesh because the number of cells per CPU core is larger in this case.

In addition, DNS calculations have been carried out to obtain information about parallel efficiency and scalability on the Cray XE6 platform on HLRS. The method for parallel computing used by OpenFOAM is known as domain decomposition, where the computational grid associated with internal cell volumes and boundary patch elements are broken into pieces and allocated to a number of processors for separate solutions. Therefore, the scale-up factor depends strongly on the number of allocated cells to each processor. Figure 4 shows the intra- (left) and inter-node (right) performance by running the DNS solver on a computational grid with two million cells. It is clear, that the intra-node speedup is far from the ideal linear speedup. This indicates that some bottleneck due to the communication between the single cores is reached. Thus, it is not worthwhile using the Cray XE6 cluster with

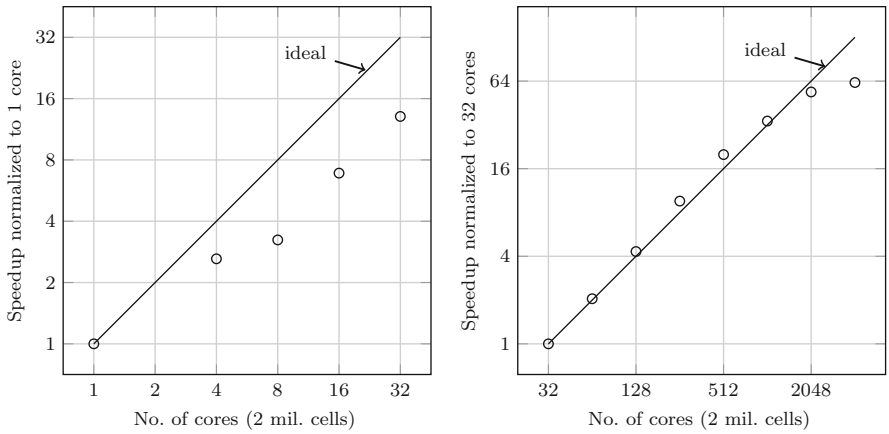

Fig. 4 Relative speedup factor by running DNS on a computational grid with two mil. cells: intra-node (*left*) and inter-node performance

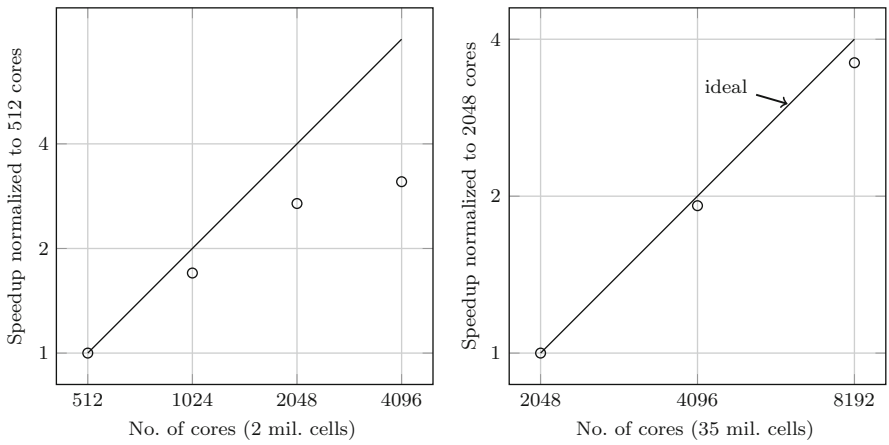

Fig. 5 Relative speedup factors by running DNS on two grids with 2 (*left*) and 35 mil. (*right*) cells

less than 32 processors on one node. On the contrary, the inter-node performance shows a very good scalability up to 2,048 processors. From 64 to 1,024 processors the scale-up is even superlinear.

Figure 5 compares the scaling performance of the DNS simulation on two different computational grids with approx. 2 million and 35 million cells. It is clear from Fig. 5 on the left that the solver does not scale well for a low number of cells per core in case of using the coarse grid. On the contrary, the scaling factor is excellent by use of the fine grid with a high number of cells per core, as one can see on the right of Fig. 5. In this case, different threads of the solver take the most time for calculation than for communication and synchronization between the CPU cores.

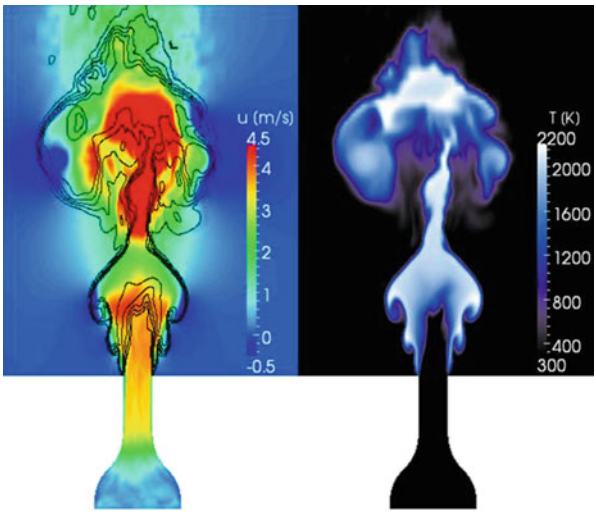

Fig. 6 Instantaneous contours of the streamwise velocity and the temperature

4 Simulation Results

4.1 Turbulent Reactive Flow

Figure 6 shows meridian planes passing through the centerline axis and being derived from the LES on the finest grid with 10.7 million nodes. The flame front is indicated by isolines of the progress variable $\tilde{\theta} = 0.1/0.3/0.5/0.7/0.9$ in contours of the streamwise velocity on the left of Fig. 6, which is corrugated and stretched by the turbulent flow. Both an inner and an outer reaction zone can be identified, which are sustained by a premixed and a non-premixed combustion. The diluted mixture is pre-burned by a higher reaction rate from the premixed combustion, the remaining fuel or combustible intermediate species (e.g. CO) mixes thereafter with ambient air leading to a weaker diffusion flame. In this case, the flame is a so-called partially premixed flame, where both premixed and non-premixed combustion regimes exist at the same time.

By passing through the convergent nozzle, the unburnt mixture is accelerated and homogenized according to continuity, so that the flow is rather undisturbed there. As a result, the premixed flame front is not strongly corrugated. At the reaction zones of the primary premixed flame, the temperature increases from 300 to 2,200 K from unburned to burned state. The resulting thermal expansion and buoyancy lead again to an acceleration of the gas. The flow is however even less turbulent due to the strongly increased fluid viscosity at high temperature. As the gradient of flow velocity and the turbulence level are relatively low, large ring vortices or coherent structures are generated in the shear layer between the main jet and the surrounding air, which contribute to the transition process from laminar to turbulent flow regime. These flow instabilities result in a strong entrainment of ambient air into the primary

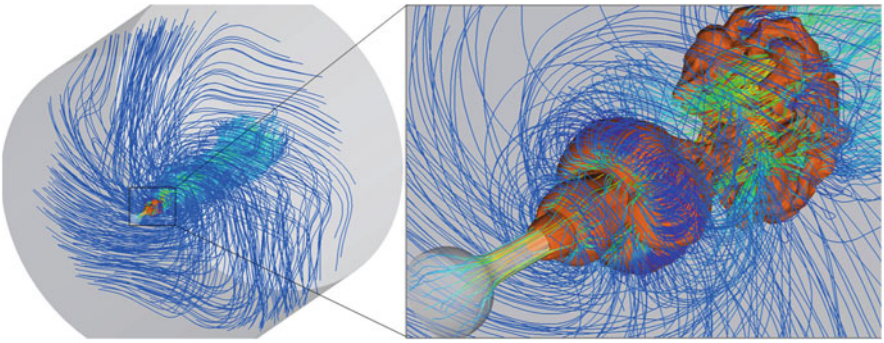

Fig. 7 Three-dimensional streamlines colored by contours of the streamwise velocity

exhaust gas, which enhance the mixing and combustion process in the secondary diffusion flame. Further downstream, the coherent vortices become unstable and break down leading to the fully turbulent flow regime.

The instantaneous three-dimensional trajectories of the flow field shown in Fig. 7 illustrate behaviors of these flow patterns clearly, where the streamlines are colored by values of the streamwise velocity and the flame surface of the external diffusion flame is indicated by isosurface of $T = 1,800\,\mathrm{K}$. On the left of Fig. 7, the surrounding air is sucked into the flame region following large-scale helical paths. Looking more closely at the near field region on the right of Fig. 7, sinks of the streamlines can be identified as the coherent ring vortices, which drive the ambient air into the secondary diffusion reaction zone. Moreover, shape of the flame surface evolves mostly with these large vortical motions as well, which is caused by interactions of the flame with the turbulent flow.

Figure 8 on the left compares intensity signals from the OH-chemiluminescence measurement which represents line-of-sight integrated values of the excited OH or OH^* concentration, with the calculated mass fraction of OH^* from DNS, which has been appropriately summed up along the lines-of-sight for each position of the diagram. Obviously, there is a qualitatively good agreement for OH^* intensity or concentrations given by both methods. The length of the flame is predicted accurately by the DNS simulation. In the following, time-mean velocities derived from the LES simulations with different grid resolutions will be compared. As the DNS calculation has only be run for 0.2 s (see Table 1) which is too short to resolve long-term coherent vortical flows, statistically converged mean fields cannot be accomplished yet for direct comparison with LES results.

4.2 Influence of Grid Resolution

Figure 9 demonstrates influence of the mesh size on the resolved time mean flow field for the LES simulation. It is obvious that the grid resolution imposes a major impact in this case where the flame length increases significantly by using a more

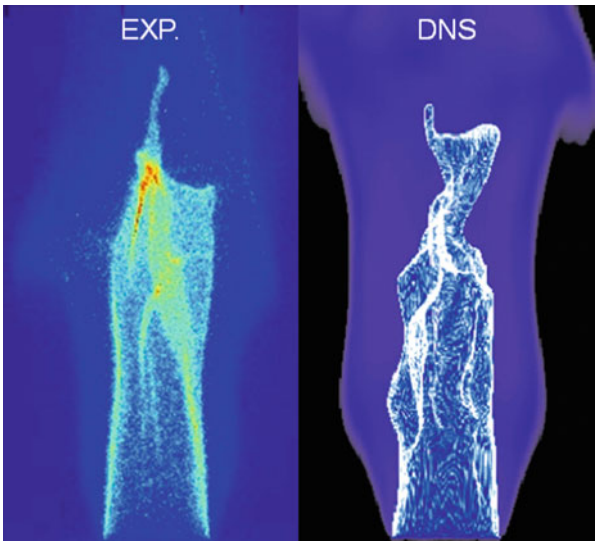

Fig. 8 Comparison of OH-chemiluminescence measurement with OH^* calculated by DNS

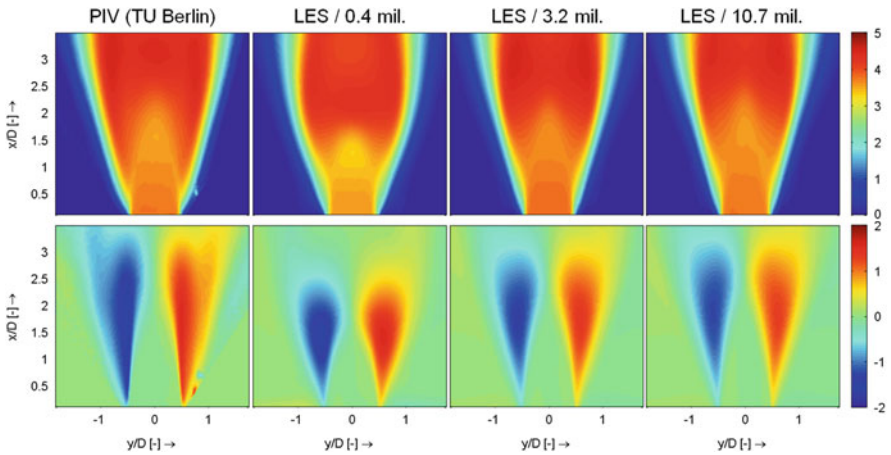

Fig. 9 Comparison of time averaged streamwise (*top*) and radial (*bottom*) velocity components derived from experiment and LES computations with different grid sizes

refined computational grid in LES. This is attributed to the fact that a smaller grid length leads to an overall attenuated turbulent diffusion ($\nu_{sgs} \propto \Delta^2$ according to the standard Smagorinsky subgrid scale model [2]) and numerical diffusion ($O(\nu_\varepsilon) \propto \Delta^2$). As shown in Fig. 9, the solution provided by LES on the finest mesh shows the best agreement with the experimental data [13], which however exhibits still a slightly shorter flame than the measured one. This difference is caused by the quasi-laminar flow nature of the considered case, where the LES fails to predict

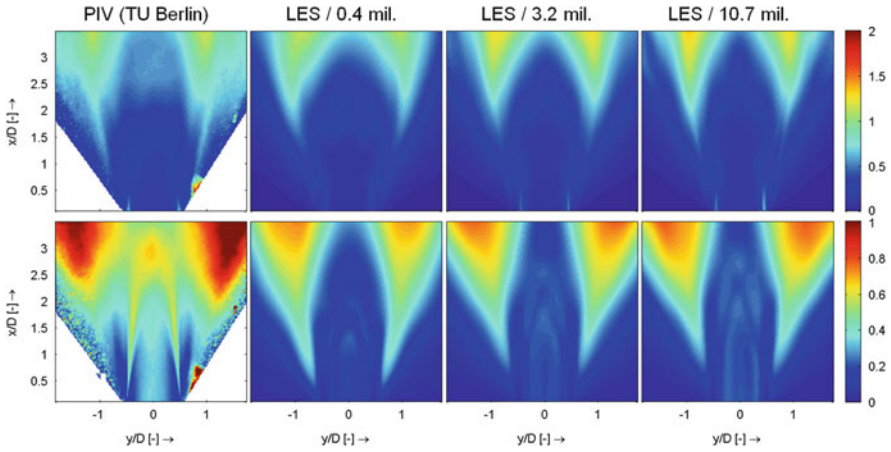

Fig. 10 Comparison of RMS streamwise (*top*) and radial (*bottom*) velocity fluctuations provided by experiment and LES computations with different grid sizes

the correct molecular transport coefficients (viscosity ν_l, thermal diffusivity a_l and diffusion coefficient D_l) used in the governing equation. Instead, the LES method applies the effective, superimposed values together with the turbulent or sgs part for these parameters, i.e. $\nu_{eff} = \nu_l + \nu_{sgs} | a_{eff} = a_l + a_{sgs} | D_{eff} = D_l + D_{sgs}$ (see Fig. 1), so that the transport fluxes are always overpredicted by the LES in regions where the flow is characterized by a laminar nature. This effect becomes weaker with a refined grid resolution, as the turbulent viscosity decreases strongly with the grid length.

A finer computational grid leads to a better resolved, thinner shear layer between the main jet and the free domain, which results in a higher gradient of the velocity and therefore a higher turbulence level. Consequently, the root mean square values (RMS) of velocity fluctuations or the roots of Reynolds stresses are generally larger in case of using a refined mesh, as shown in Fig. 10. The influence of the laminar natured coherent flow on the LES modeling applies to the calculated RMS velocity fluctuations as well, which are not as high as those from the measurement, because the turbulent transport fluxes are predicted too high. In this case, the flame front does not fluctuate as intensive as it is in the reality, so that a large difference can be identified directly in the vicinity of the flame surface (see lower part of Fig. 10).

As the compressible formulation for LES and DNS is used in the current work, the noise radiations or respectively the pressure fluctuations inside the computational domain can be directly calculated. In Fig. 11, sound pressure levels (SPL) derived from different simulation methods and the experiment show a good agreement. The DNS solution follows the measured profile very well in the whole considered frequency range. The SPLs from LES are predicted smaller than those of the DNS and the experiment in the low frequency range (up to 200 Hz). This is again attributed to the overestimated turbulent transports in the laminar, coherent flow

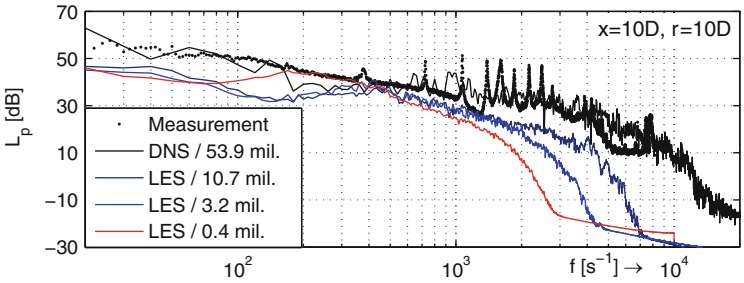

Fig. 11 SPL calculated from experiment, DNS and LES computations with different grid sizes

regions, which result in a stronger dissipation in the flow. The difference between LES and DNS is large particularly in the high frequency region. In this case, as the small scale turbulent motions can be resolved better by using a finer LES mesh, the intrinsic effect of grid refinement on the emitted sound is mostly characterized by a higher pressure level in the high frequency regions. As shown in Fig. 11, the pressure levels given by LES on different grids exhibit similar distribution in the low frequency range. However, progress of the SPLs diminishes with increasing frequencies much faster in case of using coarser computational grids.

5 Conclusions

The work presents a numerical study on LES and DNS simulations of turbulent combustion by means of different grid resolutions. The objective is to assess the influence of grid refinement on the resolved reactive flow field and the emitted noise level by means of LES combustion modeling. A realistic, moderately turbulent jet flame has been considered for this study, which was also experimentally investigated. It has been shown that the refinement of the computational grid plays an important role for predicting the combustion properties with LES, thereby the calculated length of the flame increases clearly by using a finer resolved grid due to attenuated numerical diffusion. In addition, the noise level derived from LES on a more refined grid is higher than that provided by LES on a coarse grid, this is discernible particularly in the high frequency domain. In fact, the filtering procedure implicitly employed by the LES method results in an overall enhanced numerical diffusion whose effect depends on the grid resolution, so that the predicted flame length as well as the sound level by LES is generally lower than those given by the DNS simulation. Although more computational effort is required for LES on a finer mesh, a better accuracy have been evidenced. Nevertheless, LES simulations on the coarse grids are able to reproduce the main dynamics of the flow appropriately so that they are also useful, for example, to gain a first insight of the flow patterns. With

help of the current study, a more detailed estimation for LES of turbulent combustion and its noise propagation on a further refined grid level may be accomplished.

Acknowledgements The authors gratefully acknowledge the financial support by the German Research Council (DFG) through the Research Unit DFG-BO693 "Combustion Noise". Major part of the computation time was kindly provided by the High Performance Computing Center Stuttgart (HLRS) of the University of Stuttgart and the Steinbuch Centre for Computing (SCC) of the Karlsruhe Institute of Technology.

References

1. H. Pitsch, Large-Eddy simulation of turbulent combustion. Annu. Rev. Fluid Mech. **38**, 453–482 (2006)
2. J. Fröhlich, *Large Eddy Simulation Turbulenter Strömungen* (Teubner Verlag, Wiesbaden, 2006)
3. A. Schwarz, J. Janicka (eds.), *Combustion Noise* (Springer, Berlin, 2009). ISBN-10: 3642020372
4. S. Marburg, B. Nolte (eds.), *Computational Acoustics of Noise Propagation in Fluids* (Springer, Berlin, 2008). ISBN 978-3-540-77447-1
5. H. Schmid, P. Habisreuther, W. Leuckel, A model for calculating heat release in premixed turbulent flames. Combust. Flame **113**, 79–91 (1998)
6. T. Poinsot, D. Veynante, *Theoretical and Numerical Combustion*, 2nd edn. (Edwards, Philadelphia, 2005). ISBN 978-1-930217-10-2
7. J. Kee, F. Rupley, J. Miller, Chemkin-II: a Fortran chemical kinetics package for the analysis of gas-phase chemical kinetics, Report No. SAND89-8009B, Sandia National Laboratories (1989)
8. N. Peters, *Turbulent Combustion* (Cambridge University Press, Cambridge, 2000)
9. F. Zhang, P. Habisreuther, M. Hettel, H. Bockhorn, Modelling of a premixed swirl-stabilized flame using a turbulent flame speed closure model in LES. Flow Turbul. Combust. **82**, 537–551 (2009)
10. F. Zhang, P. Habisreuther, H. Bockhorn, A unified TFC combustion model for numerical computation of turbulent gas flames, in *High Performance Computing in Science and Engineering '12*, ed. by W.E. Nagel, D.B. Kröner, M.M. Resch (Springer, Berlin, 2013). ISBN 978-3-642-33374-3
11. F. Zhang, P. Habisreuther, M. Hettel, H. Bockhorn, A newly developed unified turbulent flame speed closure (UTFC) combustion model for numerical simulation of turbulent gas flames, 25. Deutscher Flammentag, Karlsruhe, Germany (2011)
12. R.J. Kee et al., *Chemically Reacting Flow: Theory and Practice* (Wiley, New York, 2003)
13. H. Nawroth, C.O. Paschereit, F. Zhang, P. Habisreuther, H. Bockhorn, Flow investigation and acoustic measurements of an unconfined turbulent premixed jet flame, in *43rd AIAA Fluid Dynamics Conference and Exhibit*, San Diego, 2013
14. T. Kathrotia et al., Experimental and numerical study of chemiluminescent species in low-pressure flames. Appl. Phys. B **107**, 571–584 (2012)
15. OpenCFD Ltd, *OpenFOAM User Guide, Version 2.0.1* (OpenFOAM® Documentation - The OpenFOAM® Foundation, 2011). www.openfoam.org
16. J. Ferziger, M. Perič, *Computational Methods for Fluid Dynamics* (Spinger, Berlin, 2002)
17. M. Klein, A. Sadiki, J. Janicka, A digital filter based generation of inflow data for spatially developing direct numerical or large eddy simulations. J. Comput. Phys. **286**, 652–665 (2003)
18. T. Poinsot, S. Lele, Boundary conditions for direct simulation of compressible viscous flows. J. Comput. Phys. **101**, 104–129 (1992)

19. D.G. Goodwin, *Cantera C++ Users Guide* (California Institute of Technology, Pasadena, 2002)
20. F. Zhang, H. Bonart, P. Habisreuther, H. Bockhorn, Prediction of combustion generated noise using direct numerical simulation. Euromech Colloquium 546, Villa Vigoni, Menaggio, Italy, 2013
21. F. Zhang, H. Bonart, P. Habisreuther, H. Bockhorn, Direct Numerical Simulations of Turbulent Combustion with OpenFOAM. 26. Deutscher Flammentag, Duisburg (2013)
22. Karlsruhe Institute of Technology (KIT), Karlsruhe, Germany, Rechenzentrum. HP XC4000 User Guide (2009)
23. High Performance Computing Center Stuttgart (HLRS) (2011): CRAY XE6 (HERMIT), http://www.hlrs.de/systems/platforms/cray-xe6-hermit/
24. G.P. Smith, D.M. Golden, M. Frenklach, N.W. Moriarty, B. Eiteneer, M. Goldenberg, C.T. Bowman, R.K. Hanson, S. Song, W.C. Gardiner Jr., V.V. Lissianski, Z. Qin, http://www.me.berkeley.edu/gri_mech/